Numerical study of Blood Hemodynamic and Heat Transfer in Catheterized Multiple Stenosis Artery

Dr. Kadhum Audaa Jehhef
Ph.D., Department of Mechanics
Institute of Technology, Middle Technical University, Iraq
Email: kadhum.audaa@yahoo.com

Abstract

A non-Newtonian model of blood flow through an artery multiple with a mild smooth axisymmetric contraction (stenosis) centered at (x/L = 0.6, 0.7, 0.8 and 0.9) for Reynolds number values of (Re_b= 60, 80, 100 and 120) with intravascular catheter cooling is investigated numerically. Cross model chosen as blood viscosity model. The flow assumed to be steady, laminar, two-dimensional and axially symmetric. The governing equations of motion and energy in terms of the viscous shear stress and boundary conditions in cylindrical coordinate system transformed using a radial coordinate transformation before they discretized using a finite difference scheme based on central difference approximations on non-uniform grids. The present numerical results obtained in terms of blood flow and thermal characteristics shown that the friction factor increased by 52 % and the Nusselt number by 43% with increasing the stenosis height from 0 to 16.5 %. In addition, the increasing stenosis height caused to increase the dimensionless flow impedance, axial velocity and shear rate along the artery and the catheter walls. However, the presence of multi stenosis in the artery will cause to increase the impedance of the flow.

Keywords: Cross model, multi-stenosis, stenosed artery, blood flow.

1. Introduction

Blood flow through arteries is very importance because it provides an insight into physiological situations. Under diseased cases, abnormal and unnatural growth develops in the artery lumen at various locations of the cardiovascular system. Therefore, the growths of stenosis will effect on the blood flow and the blood temperatures increased in the artery. The effect of blood flow in artery with a single or multiple mild stenosis commonly occurs in the femoral and pulmonary arteries, has been studied extensively in recent years [18], [11], [6] and [14]. A mathematical solution of the steady flow of Casson fluid through an inclined artery of non-uniform cross section with multiple stenosis was developed by [19], their results showed that the flux increases with increasing yield stress in the stenosis regions. The heat transfer and fluid flow analysis of blood flow through multi stenosis arteries with viscous dissipation effects considered by [16], their result indicated that the high radial velocities prevail for high degree of stenosis and maximum velocity gradient in the concavity in artery wall. Various stenosis configurations have been

suggested by many researchers, for example, the cosine-shaped geometry was considered and analyzed with different parameters by [10] and [4]. Also, a composite shaped geometry of arterial stenosis is suggested by [9]. In these studies, the shape of stenosis was considered symmetrical about the axis as well as radius of the flow cylinder. However, [20] and [1] studied the model of blood flow through an artery for improved generalized geometry of multiple stenosis located at equispaced points. In small vessels, blood exhibits shear-dependent viscosity and requires a finite yield stress before flow can commence, thereby making the non-Newtonian nature [2]. The Power-law fluid showed far more non-Newtonian influence was experimentally founded by [17]. A number of researchers have studied the flow of non-Newtonian fluids such as in [23] with various perspectives. [15] presented a numerical study of a non-Newtonian pulsatile model of blood flow through multiple stenosis with irregular surfaces. The study of blood flow in catheterized artery was considered by [13], they used micropolar fluid (fluids with suspension nature) in an annular region with constriction. The flow of couple stress fluid in an annulus with multiple constrictions at the outer wall was considered by [5]. The heat and mass transfer phenomena in the arteries and biological tissues has been investigated by [2], and [24] they developed a mathematical model

describing the dynamic response of heat and mass transfer in blood through bifurcated arteries under stenotic condition. [22] used the flow and energy equations together with the boundary conditions in dimensionless form by formulation the problem in term of vorticity- stream function model. Flow of blood through narrow stenotic vessel by considering blood as Bingham plastic fluid and shown that resistance to flow and wall shear stress increase with the size of stenosis but these increases are smaller due to the non-Newtonian nature of blood [3]. [25] represented an unsteady blood flow through constricted artery in the presence of velocity slip. Finally, [29] developed a mathematical model for studying the effect of body acceleration on pulsatile blood flow through a catheterized artery with an axially non-symmetrical mild stenosis. The aim of this study is to investigate the fluid flow and heat transfer in a multiple stenosis in catheterized artery. This study numerically investigated the effects of catheter temperature, number of stenosis and stenosis heights, on the temperature and velocity profile, impedance, wall shear stress, heat transfer coefficient and friction factor along the artery wall.

2. Mathematical Model and Numerical Solution

The uniform blood vessel segment having a multiple stenosis in its lumen is modeled as a thin rigid tube with a

circular cross-section containing an incompressible non-Newtonian characterized by Cross model and assume that the artery wall at constant body temperature of (T_b =37 °C) and the catheter, but the cooling catheter surface maintained at specified constant wall temperature (T_c). Let two dimensional of (r, x) be the coordinates in the cylindrical polar coordinates system where the (x-axis) is taken along the axis of the artery while with centered catheter segment shown in (**Fig. 1**).
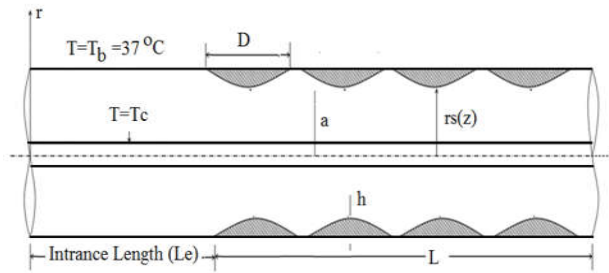
Fig.1 Schematic diagram of catheterized multiple stenosed artery.

The vessel has a circular cross section whose radius is R_o in everywhere except in a multiple small regions centered at (x/L = 0.6, 0.7, 0.8 and 0.9) with a mild smooth axisymmetric contraction (stenosis), described by following function [18]:

$$R = R_o \left(St \left(\frac{1 - \cos(\pi x / D)}{2} \right)^2 \right), \quad 0 \le x \le 2D$$

(1)

where St is the stenosis degree defined by:

$$St = 1 - \frac{R_o - R_{min}}{R_o} \cdot 100\% \quad (2)$$

R_{min} is the artery radius at the throat of stenosis constriction. By using the non-Newtonian model constitutive equation of the Cross model by [21]:

$$\mu(\dot{\gamma}) = \mu_\infty + \frac{\mu_0 - \mu_\infty}{1 + (m \dot{\gamma})^n}$$

(3)

Where μ_o=0.056, μ_∞=0.0345 Pas, m=1.007s and n=0.285

2.1 Governing Equations

The governing equations for the x and r components of momentum together with the equation of continuity, in the cylindrical coordinate system may be as [26]:

The continuity equation:

$$\frac{1}{r} \frac{\partial (ru)}{\partial r} + \frac{\partial v}{\partial x} = 0$$

(4)

r-momentum equation:

$$u \frac{\partial v}{\partial x} + v \frac{\partial v}{\partial r} = -\frac{1}{\rho} \frac{\partial p}{\partial r} +$$

$$2v \left[\left(\frac{\partial^2 v}{\partial x^2} + \frac{\partial^2 v}{\partial r^2} + \frac{1}{r} \frac{\partial v}{\partial r} - \frac{v}{r^2} \right) + \frac{\partial \mu}{\partial x} \left(\frac{\partial v}{\partial x} + \frac{\partial u}{\partial r} \right) + 2 \frac{\partial \mu}{\partial r} \frac{\partial v}{\partial r} \right]$$

(5)

x-momentum equation:

$$u \frac{\partial u}{\partial x} + v \frac{\partial u}{\partial r} = -\frac{1}{\rho} \frac{\partial p}{\partial x} +$$

$$v \left[\left(\frac{\partial^2 u}{\partial x^2} + \frac{\partial^2 u}{\partial r^2} + \frac{1}{r} \frac{\partial u}{\partial r} \right) + \frac{\partial \mu}{\partial r} \left(\frac{\partial v}{\partial x} + \frac{\partial u}{\partial r} \right) + 2 \frac{\partial \mu}{\partial x} \frac{\partial u}{\partial x} \right]$$

(6)

energy equation:

$$\rho C_p \left(u \frac{\partial T}{\partial r} + v \frac{\partial T}{\partial x} \right) = k \left[\frac{1}{r} \frac{\partial}{\partial r} \left(r \frac{\partial T}{\partial r} \right) + \frac{\partial}{\partial x} \left(\frac{\partial T}{\partial x} \right) \right]$$

(7)

where u and v are the components of velocity in r and x directions respectively.

Let us now introduce a set of non-dimensional variables:

$$R = \frac{r}{R_o}, \; X = \frac{x}{L}, \; U = \frac{u}{U_o}, \; V = \frac{v}{U_o},$$

$$P = \frac{p}{\rho U_o^2}, \; \theta = \frac{T - T_{in}}{T_c - T_{in}}, \; Pr = \frac{\nu}{\alpha}$$

where U_o is the velocity averaged over the section of radius R_o. Moreover, the Reynolds number can be defined as:

$$Re = \frac{\rho R_o U_o}{\mu_\infty}$$

Dimensionless Continuity Equation:

$$\frac{1}{R}\frac{\partial(RU)}{\partial R} + \frac{\partial(V)}{\partial X} = 0$$

(8)

Dimensionless r-momentum equation:

$$U\frac{\partial V}{\partial X} + V\frac{\partial V}{\partial R} = -\frac{1}{\rho}\frac{\partial P}{\partial R} +$$

$$2\frac{\delta}{Re}\left[(\frac{\partial^2 V}{\partial X^2} + \frac{\partial^2 V}{\partial R^2} + \frac{1}{R}\frac{\partial V}{\partial R} - \frac{V}{R^2}) + \frac{\partial \mu}{\partial X}(\frac{\partial V}{\partial X} + \frac{\partial U}{\partial R}) + 2\frac{\partial \mu}{\partial R}\frac{\partial V}{\partial R}\right]$$

(9)

Dimensionless x-momentum equation:

$$U\frac{\partial U}{\partial X} + V\frac{\partial U}{\partial R} = -\frac{1}{\rho}\frac{\partial P}{\partial X} +$$

$$\frac{\delta}{Re}\left[(\frac{\partial^2 U}{\partial X^2} + \frac{\partial^2 U}{\partial R^2} + \frac{1}{R}\frac{\partial U}{\partial R}) + \frac{\partial \mu}{\partial R}(\frac{\partial V}{\partial X} + \frac{\partial U}{\partial R}) + 2\frac{\partial \mu}{\partial X}\frac{\partial U}{\partial X}\right]$$

(10)

Dimensionless energy equation:

$$U\frac{\partial \theta}{\partial R} + V\frac{\partial \theta}{\partial Z} = \frac{k}{Re Pr}\left[\frac{1}{R}\frac{\partial}{\partial R}\left(R\frac{\partial \theta}{\partial R}\right) + \frac{\partial^2 \theta}{\partial Z^2}\right]$$

(11)

The following relation between velocity components and vorticity-stream function holds:

$$\omega = \frac{\partial v}{\partial x} - \frac{\partial u}{\partial r}, \qquad u = -\frac{1}{r}\frac{\partial \psi}{\partial x}, \; v = \frac{1}{r}\frac{\partial \psi}{\partial r}$$

(12)

The non-dimensional counterparts of the Eqs. (5 and 6) are cross differentiated and subtracted, to obtain the vorticity–stream function formulation with ω the azimuthal vorticity and ψ the Stokes stream function:

$$\left(\frac{1}{r}\frac{\partial \psi}{\partial r}\frac{\partial \omega}{\partial x} - \frac{1}{r}\frac{\partial \psi}{\partial x}\frac{\partial \omega}{\partial r}\right) + \frac{\omega}{r^2}\frac{\partial \psi}{\partial x} =$$

$$\frac{1}{Re^2}\left[\chi\left(\frac{\partial^2 \omega}{\partial x^2} + \frac{\partial^2 \omega}{\partial r^2} + \frac{1}{r}\frac{\partial \omega}{\partial r} - \frac{\omega}{r^2}\right) + 2\frac{\partial \chi}{\partial x}\frac{\partial \omega}{\partial x}\right.$$

$$+ \frac{\partial \chi}{\partial r}\left(2\frac{\partial \omega}{\partial r} + \frac{\omega}{r}\right) + 2\frac{\partial^2 \chi}{\partial r \partial x}\left(\frac{1}{r^2}\frac{\partial \psi}{\partial x} - \frac{2}{r}\; 2\frac{\partial^2 \psi}{\partial r \partial x}\right)$$

$$\left. + \left(\frac{\partial^2 \chi}{\partial x^2} - \frac{\partial^2 \chi}{\partial r^2}\right)\left(\frac{1}{r}\frac{\partial^2 \psi}{\partial r^2} - \frac{1}{r}\frac{\partial^2 \psi}{\partial x^2} - \frac{1}{r^2}\frac{\partial \psi}{\partial r}\right)\right]$$

(13)

where the dimensionless form of the blood viscosity was given by [29]:

$$\dot{X}(\gamma) = 1 + \frac{(\delta - 1)}{1 + (\Lambda \dot{\gamma})^{1-n}}$$

(14)

Where the dimensionless variables given by:

$$\dot{X} = \frac{\mu}{\mu_\infty}, \qquad \delta = \frac{\mu_0}{\mu_\infty}, \qquad \Lambda \rightarrow \frac{\Lambda U_o}{R_o}$$

In addition, the blood shear rate defined as:

$$\dot{\gamma}^2 = \frac{4}{r^2}\left[\frac{1}{r^2}\left(\frac{\partial \psi}{\partial x}\right)^2 + \left(\frac{\partial^2 \psi}{\partial r \partial x}\right)^2 - \frac{1}{r}\frac{\partial \psi}{\partial x}\frac{\partial^2 \psi}{\partial r \partial x}\right] +$$

$$\frac{1}{r^2}\left(\frac{\partial^2 \psi}{\partial r^2} - \frac{1}{r}\frac{\partial \psi}{\partial r} - \frac{\partial^2 \psi}{\partial x^2}\right)^2$$

(15)

The relation between the vorticity and stream function are related by the Poisson equation:

$$-\omega r = \frac{\partial^2 \psi}{\partial x^2} + \frac{\partial^2 \psi}{\partial r^2} - \frac{1}{r}\frac{\partial \psi}{\partial r} \quad (16)$$

2.2 Grid Generation

The grid generation in which grid line coincides with the body contour in the flow region can provide an accurate representation of boundary conditions in the region of greatest sensitivity. [12] introduced a method for numerical generation of curvilinear coordinate systems with coordinate line conformal with all boundaries of arbitrarily shaped bodies in a two – dimensional flow region. In the method, the polar coordinate (x,r) of the boundary grid generation points in complex physical space are computed as solution of an elliptic system of partial differential equations with Dirichlet boundary conditions. In this work, two different sets of partial differential equations are used in boundary grid generation (ζ,η).[30] proposed Poisson's equation as the coordinate generating system. It is:

$$\xi_{xx} + \xi_{rr} = P(\zeta,\eta) \qquad\qquad (17)$$

$$\eta_{xx} + \eta_{rr} = Q(\zeta,\eta) \qquad\qquad (18)$$

This yields an elliptic system of quasilinear equations in the transformed plane:

$$\alpha x_{\zeta\zeta} - 2\beta x_{\zeta\eta} + \gamma x_{\eta\eta} = -J^2\left(P(\zeta,\eta)x_\zeta + Q(\zeta,\eta)x_\eta\right)$$
(20)

$$\alpha r_{\zeta\zeta} - 2\beta r_{\zeta\eta} + \gamma r_{\eta\eta} = -J^2\left(P(\zeta,\eta)r_\zeta + Q(\zeta,\eta)r_\eta\right)$$
(21)

where α , β and γ are transformation coefficients

$$\left.\begin{array}{l} \alpha = x_\eta^2 + r_\eta^2 \\[4pt] \beta = x_\zeta\ x_\eta + r_\zeta\ r_\eta \\[4pt] \gamma = x_\zeta^2 + r_\zeta^2 \end{array}\right\} \quad (22)$$

Control of the coordinate line spacing in the field and on the boundary if Neumann boundary conditions are imposed, can be accomplished through the control functions $P(\zeta,\eta)$ and $Q(\zeta,\eta)$.

and J denotes the Jacobain of the transformation

$$J = \frac{\partial(x,r)}{\partial(\zeta,\eta)} = x_\zeta\ r_\eta - x_\eta\ r_\zeta \quad (23)$$

The constant ζ lines and constant η lines can be spaced as desired around the boundaries in the physical domain, since the assignment of the (ζ,η) values to (x,r) boundary points via (x_i) and (r_i) functions are arbitrary.

2.3   Generalized   Coordinate Transformation

In this section the relationships between the physical coordinate (x,r) and the computational coordinate (ζ,η) will be established. First it is assumed that there is a unique, single valued relationship between the generalized coordinates and the physical coordinates, the transformation relating the physical space and the computational space is specified by the direct transformation [27]:

$$\zeta = \zeta(x,r) \quad , \qquad \eta = \eta(x,r) \ (24)$$

The transformation from computational space to the physical space is specified by the inverse transformation [27]:

$$x = x(\zeta, \eta) \quad , \qquad r = r(\zeta, \eta) \quad (25)$$

The determination of the coordinate transformation is called grid generation. Once the coordinate transformation has been determined the differential equations must be transformed from physical space (x,r) into computational space (ζ,η). Given the functional relationships of Eqs. (24 and 25), the governing equation can be transformed into corresponding equations containing partial derivatives with respect to ζ and η.

Eqs. (24 and 25) can now be solved on a uniform grid in computational plane. The derivatives of (ζ_x) , (η_x) , (ζ_r) and (η_r) are called the metrics of the direct transformation. The Jacobain determinate J is defined:

$$J = \frac{\partial(x,r)}{\partial(\zeta,\eta)} \quad (26)$$

It can be shown that the metrics of the direct transformation can be expressed as [28]:

$$\left. \begin{array}{ll} \zeta_x = \dfrac{r_\eta}{J}_{X/R} , & \zeta_r = -\dfrac{x_\eta}{J} \\[2mm] \eta_x = -\dfrac{r_\zeta}{J} , & \eta_r = \dfrac{x_\zeta}{J} \end{array} \right\} \quad (27)$$

After identifying lines of symmetry and establishing the nodal network for the system, the appropriate finite difference equation was written for each node working with the equation defining for example the vorticity Eq. (16) will be written as:

$$-\omega r = \left(\lambda \frac{\partial \psi}{\partial \zeta} + \sigma \frac{\partial \psi}{\partial \zeta} + \alpha \frac{\partial^2 \psi}{\partial \zeta^2} - 2\beta \frac{\partial^2 \psi}{\partial \zeta \partial \zeta} + \gamma \frac{\partial^2 \psi}{\partial \zeta^2} \right) \Big/ J -$$
$$\frac{1}{r} \left[\frac{\partial \psi}{\partial \eta} \frac{\partial x}{\partial \zeta} - \frac{\partial \psi}{\partial \zeta} \frac{\partial x}{\partial \eta} \right] \Big/ J$$
$$(28)$$

To transform Eq. (12) then it has been divided to several partitions:

$$u = -\frac{1}{r} \frac{\partial \psi}{\partial x} = \frac{-1}{r} \left(\frac{\partial \psi}{\partial \zeta} \frac{\partial r}{\partial \eta} - \frac{\partial \psi}{\partial \zeta} \frac{\partial r}{\partial \zeta} \right) / J$$
$$(29)$$

$$v = \frac{1}{r} \frac{\partial \psi}{\partial r} = \frac{1}{r} \left(\frac{\partial \psi}{\partial \eta} \frac{\partial x}{\partial \zeta} - \frac{\partial \psi}{\partial \zeta} \frac{\partial x}{\partial \eta} \right) / J$$
$$(30)$$

In this study the following thermo-physical properties of adult human blood were presented in (**Table.1**).

Table .1 Standard properties human blood (37 °C) [8]

Physical Properties	Values	Units
Density	1064	(kg/m^3)
Specific heat	3840	(J/kg. K)
Thermal	0.53	(W/m.K)
conductivity	0.0045	(kg/s.m)
Viscosity		

2.4 Initial and Boundary Conditions

At inlet cross section of the artery for boundary at (x=0) given by:

$$u(0,r) = Uo, \quad v(0,r) = 0, \quad T(0,r) = T_{in}$$

Also, at outlet cross section (x=L) assumed the following boundary conditions:

$$v(L,r) = 0, \quad \frac{\partial u(L,r)}{\partial x} = 0, \quad \frac{\partial T(L,r)}{\partial x} = 0$$

However, at outer and inner pipe walls, no slip boundary condition for the blood flow velocity as the following:

$v(x, R_i) = 0$, $u(x, R_i) = 0$, $v(x, R_o) = 0$, $u(x, R_o) = 0$

It was assumed that there is an isotherm uniform temperature on inner catheter cooling wall as:

$T(x, R_i) = T_c$

The artery wall maintained at constant temperature of the body temperature.

$T(x, R_o) = T_b = 37\,^O C$

The boundary conditions are required for all boundaries of computational domain since the governing equations are elliptic in partial coordinates, see the Fig. (2a).

1- In the inlet the stream function and vorticity set as zero value.
2- On the walls of the artery and the cooling catheter, the value of the stream function is unity, corresponding to an impermeable wall.
3- The value of vorticity on the walls of the artery and the cooling catheter is unknown and must be solved as a part of solution.
4- The outlet boundary of stream and vorticity which is located three periods downstream is imposed to be the same in the stream wise direction.
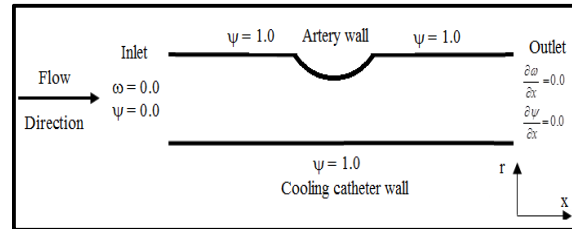
Fig.2.a Boundary condition

2.5 Numerical Method

Generally, the analytical solution for the physical domain shown in **Fig.2b** is very difficult, this is because biological phenomena often involve nonlinear partial differential equations (PDEs), but the numerical solutions of these equations are possible and easy. FDM is an approximation that converts the partial derivatives of PDEs to algebraic equations by using finite difference expressions. The continuous domain is represented by a finite-difference grids, by replacing Ø(x, r) by Ø(iΔx, jΔr) points could be located according to values of (i) and (j), general points (i, j). The computational domains and Grid used for annulus space numerical grid (i=141, j=51) **Fig 2c**. The convergence criterion for velocity is the maximum relative mass residual of the control volumes is less than 1.0 ×10⁻⁵, and the criterion for temperature is the relative difference between the two heat transfer rates obtained from two iterations separated by 1000 successive iterations by using the optimum Gauss-Seidel method and was designed to enhance fast convergence

used in this study. To improve the rate of convergence, the residual is multiplied by some terms and add that to $\psi_{(i,j)}$ at the (nth) iteration to get new $\psi_{(i,j)}^{n}$ at ((n+1)th) iteration, thus.

$$\psi_{(i,j)}^{n+1} = \psi_{(i,j)}^{n} + RF \cdot \frac{E_{(i,j)}^{n}}{2(1/(\Delta x)^2 + 1/(\Delta r)^2)} \quad (37)$$
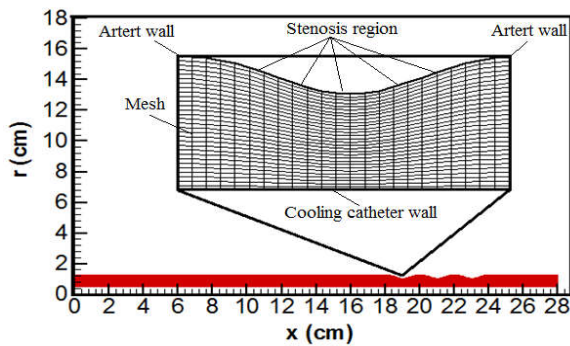
Fig.2.b: Schematic of computational domains and grid used annulus (i=141, j=51).

The parameter (RF) is called relaxation factor. The value of (RF) lies between 1 and 2, (When RF >1, the method is called successive over-relaxation SOR). Its suitable value must be found by trail-and-error. The process continues until converge criteria, $\varepsilon_{(i,j)}$, have been relaxed to values that are small enough to insure achievement of the desired accuracy. The converge criteria is as follows [30]:

$$\varepsilon_{(i,j)} = \frac{E_{(i,j)}}{2(1/(\Delta x)^2 + 1/(\Delta r)^2)} \quad (38)$$
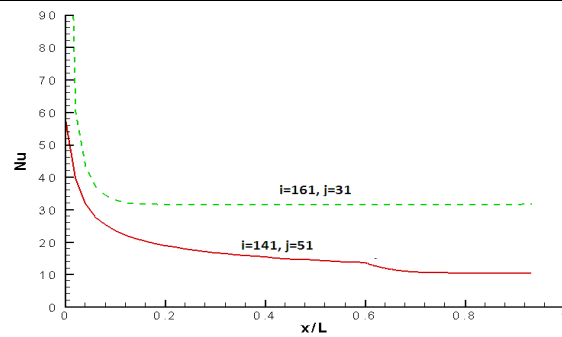
**Fig.2.c effect of grid used on the local Nusselt number versus Dimensionless axial distance.**

3. Results and Discussion

The numerical computations of the desired quantities of major physiological significance used the following parameter values: stenosis height (a=1.2 cm), inner radius (R_i=0.5 cm), outer radius (R_o=1.2 cm), the artery length (L=18 cm), entrance length (Le=12 cm), x-axis interval Δx=0.0025, r-axis interval Δr= 0.000175, Reynolds numbers (Re_b=60, 80, 100, 120), stenosis minimum radius (R_{min}=0.7, 0.8, 0.9, 1.0, 1.1, 1.2 (no stenosis)), catheter wall temperature (T_c=32 ^{o}C) and number of stenosis (No.=0, 1, 2, 3, 4). The results appeared to converge with an accuracy of the order (10^{-5}). The computed results obtained following the above mentioned method for various physical quantities of major physiological significance in order to have their quantitative measures.

The results for the axial velocity profile of the blood characterized by the generalized Cross model (non-Newtonian) at a specific location in the

stenotic region were illustrated in **Fig.3** at three regions of the catheterized artery of (a) Just before stenosis region (x/L=0.58), (b) middle stenosis region (x/L=0.6), (c) Just before stenosis region (x/L=0.62). These curves are to be analogous in the sense, showed that it decreases from their individual maximal value at the center of the annulus as moves away from it and finally drop to zero on the inner catheter cooling and outer artery wall surfaces. The axial velocity profile assumes a flat shape in the presence of stenosis instead of a parabolic one for non-stenosis artery. Thus, the presence of stenosis influence on the axial velocity of the streaming blood past a stenosed artery significantly. Moreover, show that the velocity in the middle of stenosis region increased as compared with the other regions and this increasing of velocity will decrease by using two or three stenosis instead of one stenosis due to increasing the resistance of the flow with increasing the number of the stenosis.
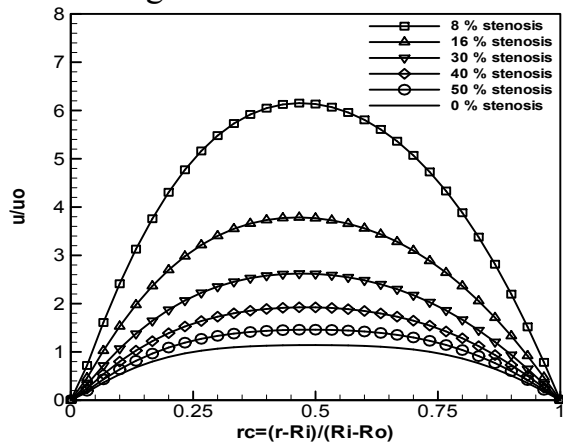

(ii) Number of stenosis=1

(iii) Number of stenosis=2

(iv) Number of stenosis=3
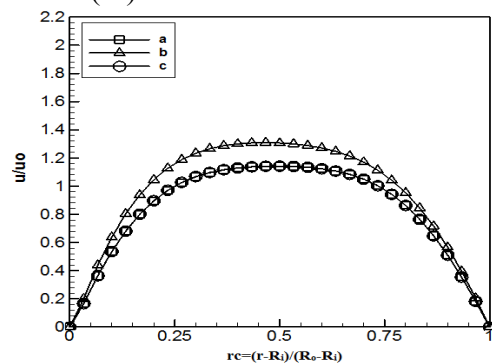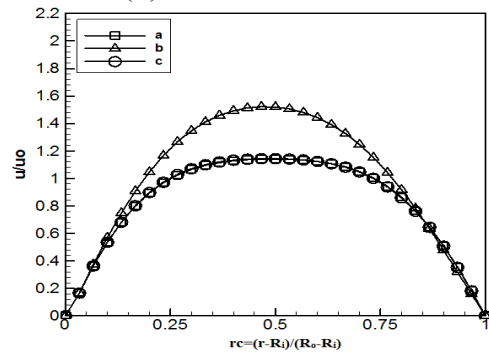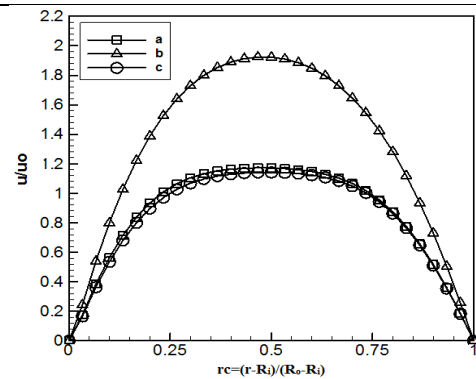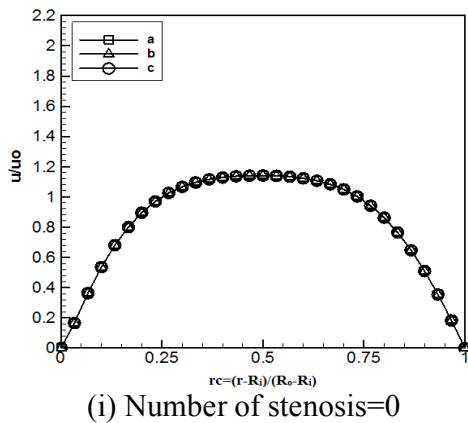
Fig.3 The dimensionless velocity for (a) Just before stenosis region (x/L=0.58), (b) middle stenosis region (x/L=0.6), (c) Just before stenosis region (x/L=0.62).

In addition, the results presented in **Fig.4** indicated that the effects of increased the stenosis height on the behaviour of blood axial velocity and the shear stress across the annular region for middle stenosis region at

(i) Number of stenosis=0

(x/L=0.6). It shows that the velocity increased with increasing the stenosis ratio from 0% no stenosis to 50% stenosis due to decreasing the area of blood flow with increasing the high of the stenosis and this will increase a resistance to the blood flow as plotted in **Fig.4 (i)**. However, the effect of stenosis height on the shear stress presented **Fig.4 (ii)**, it shows that the increased the stenosis height will increase the wall shear stress along the two walls (artery and catheter wall)**.** Moreover, show that the shear stress on the inner wall (catheter wall) is higher magnitude than that on the outer wall (artery wall) at using Cross non-Newtonian fluids, due to shear stress profile is non-linear and the velocity profile is not symmetric about the midpoint in a concentric annulus. Clearly, can show that the location of maximum velocity is closer to the inner wall than the outer wall outer wall, this was due to the high shear stress along the inner wall compared with low shear stress along the outer wall.


(i) Velocity
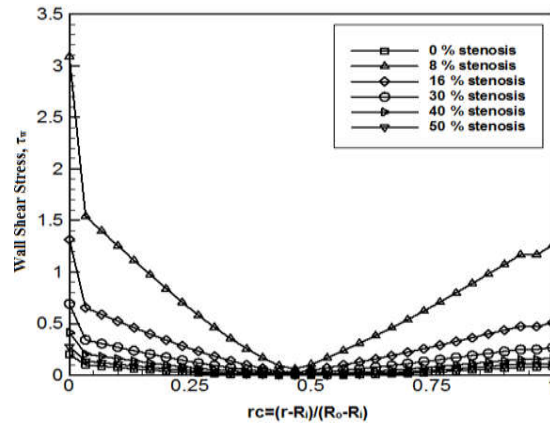
(ii) Shear stress

Fig.4: Effect of stenosis height percent on the dimensionless velocity and shear stress (x/L=0.6).
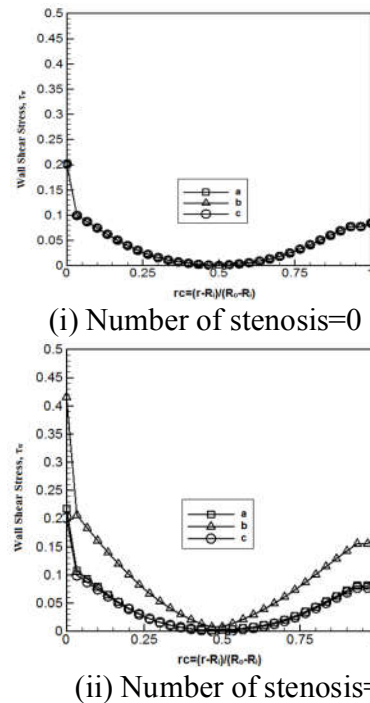
The effects of stenosis number on the dimensionless temperature distribution in the annular space between the adiabatic blood artery wall and the cooling catheter wall at 32 °C was illustrated in **Fig.5**. It shows that the temperatures will be decreasing towered the cooling catheter, but the temperatures in the middle stenosis region at (x/L=0.6) is higher than the just after stenosis region at (x/L=0.62). But, it gives smaller than the just before stenosis region at (x/L=0.58) due to increasing the velocity in the region under the stenosis. These temperatures will be increased with increasing the number of stenosis due to reusing the velocity in the region under the stenosis.

(i) Number of stenosis=0

(ii) Number of stenosis=1

(iii) Number of stenosis=0

(iv) Number of stenosis=1
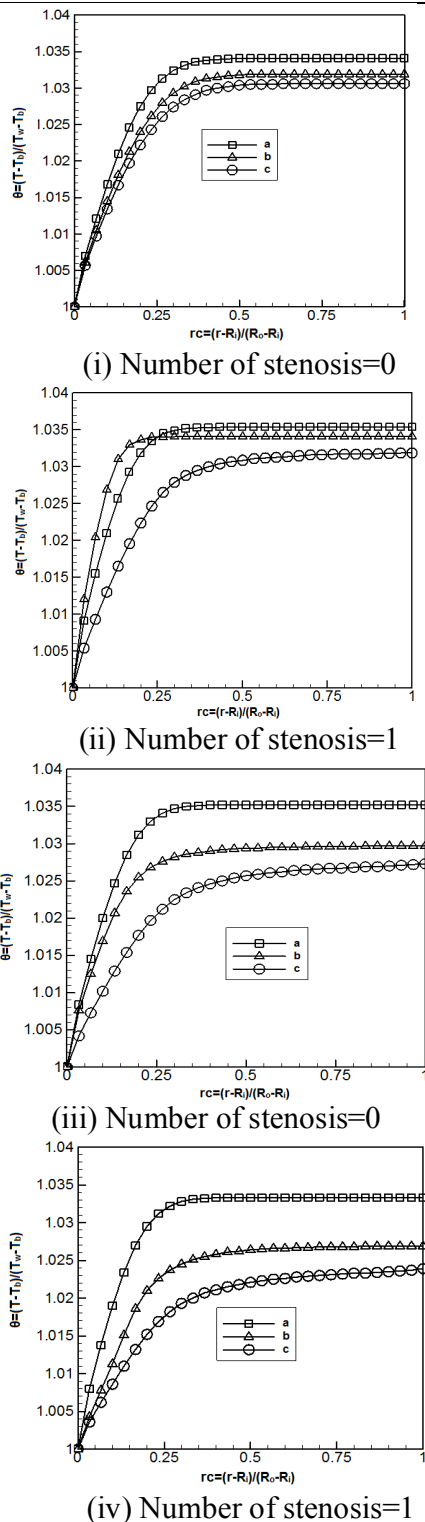
Fig.5 The dimensionless temperatures for (a) Just before stenosis region (x/L=0.58), (b)

**middle** stenosis region (x/L=0.6), (c) Just after stenosis region (x/L=0.62).

Fig.6 shows the increasing in the shear stress with using one stenosis in the region of middle stenosis region at (x/L=0.6), due to increase the velocity gradient near the wall of the stenosis and the catheter cooling wall. In addition, the increased wall shear stress will cause high defect on the endothelial cells of the artery. Shear stress is a particularly important concept in the blood hemodynamic. Blood is a living fluid, and if the forces applied to the fluid are sufficient, the resulting shearing stress can destroy red blood cells.

(i) Number of stenosis=0

(ii) Number of stenosis=1

Fig.6 The wall shear stress for (a) Just before stenosis region (x/L=0.58), (b) middle stenosis region (x/L=0.6), (c) Just before stenosis region(x/L=0.62)
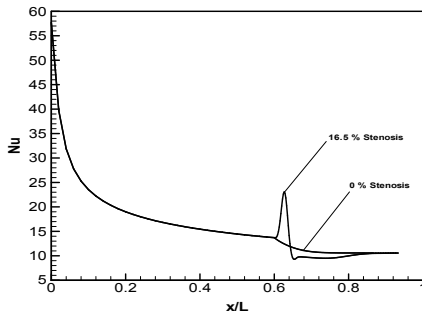
Fig. 7 shows that the effect of stenosis number on the dimensionless flow impedance (R_{min}=0.5). It shows that the values of the dimensionless flow impedance seem constant as along as the length of the artery for all numbers of stenosis. However, the impedance suddenly increases and fluctuating in the middle of the stenosis due to decrease the cross section of the artery.
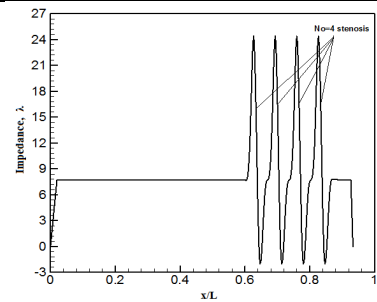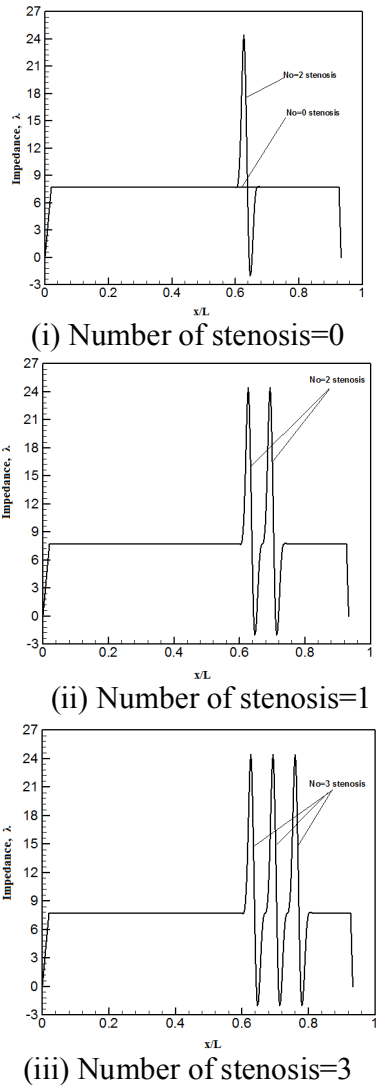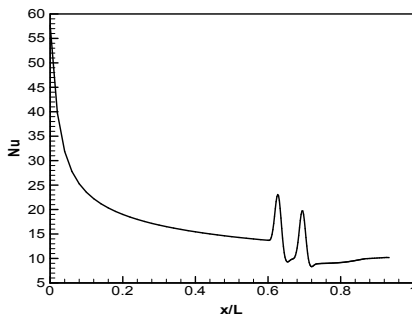

(iv) Number of stenosis=4

Fig.7: Effect of number of stenosis on the dimensionless flow impedance (rc=0.5)

(i) Number of stenosis=0

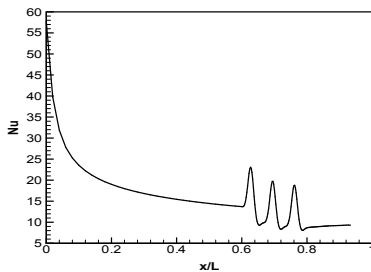(ii) Number of stenosis=1

(iii) Number of stenosis=3

Furthermore, the study of heat transfer in blood flow in stenosis artery caused by presence of stenosis in the wall artery and its effects on the Nusselt number was illustrated in **Fig. 8**. The results show that the Nusselt number will gradually decrease from the inlet of the artery due to the entrance length effect until reached the developing region in the middle length of the artery. Moreover, it refers to the effect of stenosis number on the Nusselt number at Reynolds number of (Re=60). **Fig 8i** illustrated that the Nu increase by (42%) if the stenosis high increases (from 0 to 16.5%). In addition, the results show that the values of Nu suddenly increased and then it fluctuated in the regions of the stenosis due to decreasing the cross section of the artery. This will lead to increase the blood velocity in this region and increase the heat transfer coefficient in these regions.
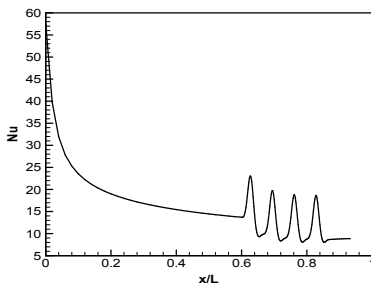
(i) Number of stenosis=0

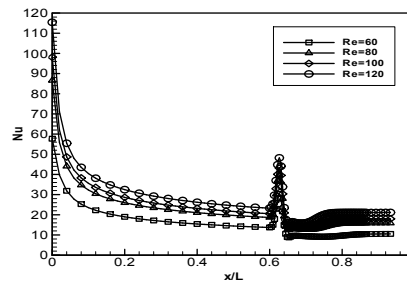(ii) Number of stenosis=1
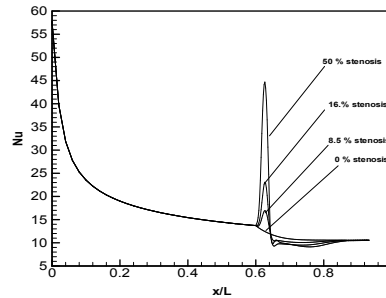

(iii) Number of stenosis=3

(iv) Number of stenosis=4

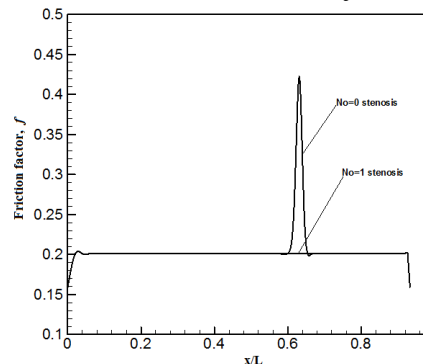**Fig.8 Effect of number of stenosis on the blood Nusselt number.**

The stenosis high and blood Reynolds number plotted in **Fig.9**. It shows that the increasing stenosis height will increase the shut of the peak Nusselt number rapidly. Also, the Nusselt number increased with increasing the Reynolds number


Fig.9 Effect of stenosis high percent on the blood Nusselt number.

Now at the same flow condition, the study of the effect of high and number of stenosis artery on the blood friction factor at (rc=R), Re=60, T_c= 32 $^{\circ}$C illustrated in **Fig. 10**. The results show that the blood friction factor will steady at 0.2 for all cases at the inlet of the artery.


(i) Number of stenosis=0

(ii) Number of stenosis=1

(iii) Number of stenosis=3

(iv) Number of stenosis=4
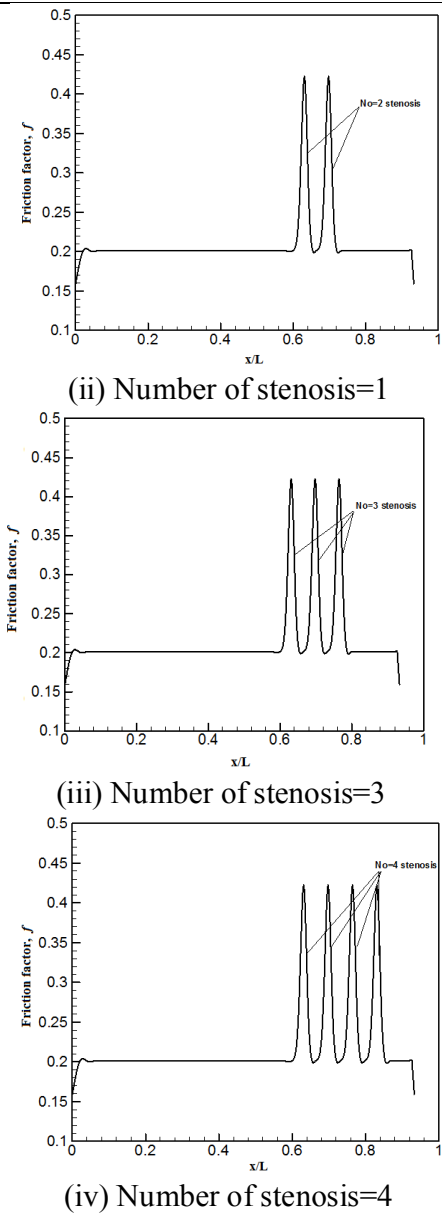
**Fig.10 Effect of number of stenosis on the friction factor for (rc=Ro).**

Nevertheless, the friction factor will increase suddenly from (0.2 to 0.4) in the stenosis region due to decreasing the cross section of the artery, this lead to increase the blood velocity in this region, this cause to increase the wall shear stress along the artery, and by

very long-term effects on the vascular remodeling, endothelial damage, changes in barrier function, and atherosclerosis. The effect of stenosis height on the blood velocity contour in the artery was presented in **Fig.11**.
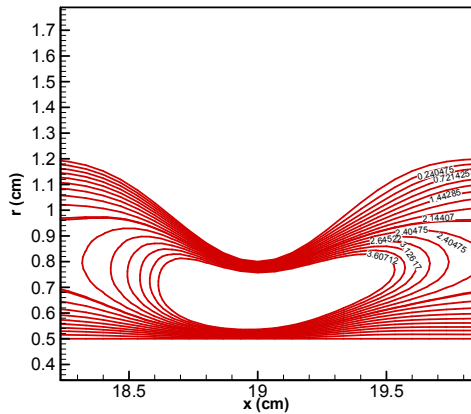

(i) 0% Stenosis

(ii) 8% Stenosis

(iii) 16% Stenosis
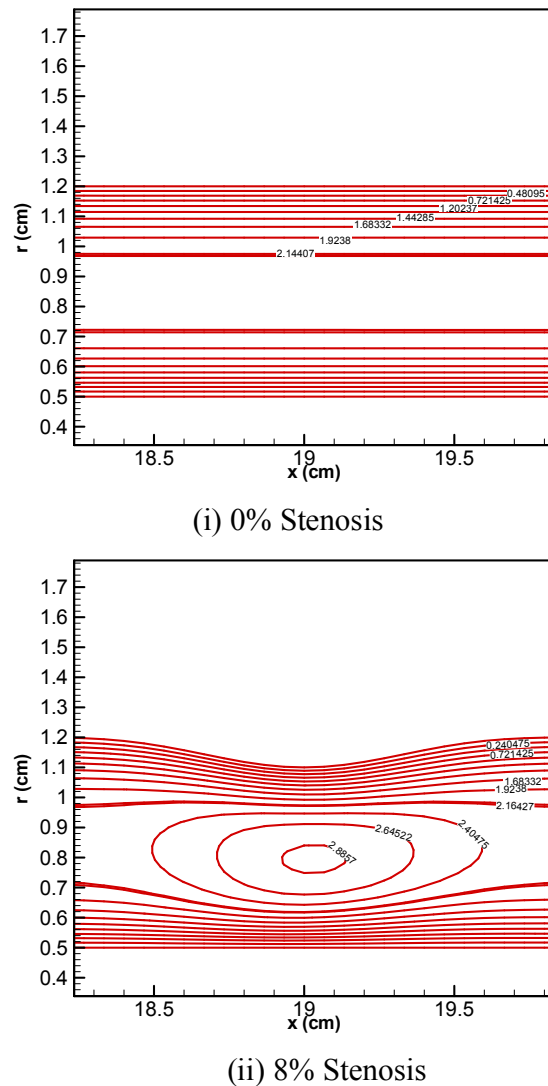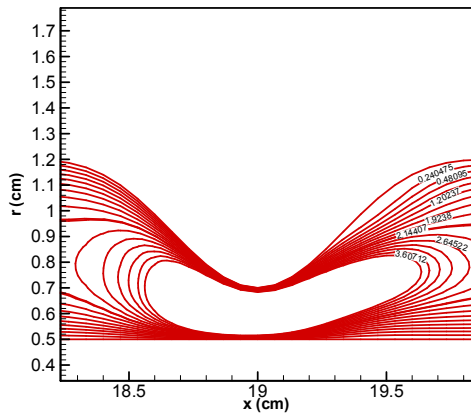
(iv) 30% Stenosis
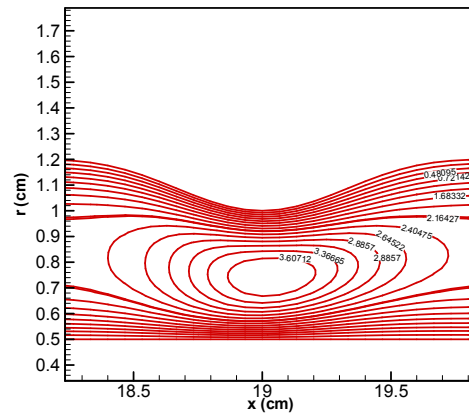
(v) 40% Stenosis

(vi) 50% Stenosis

Fig.11 Effect of stenosis high percent on the blood velocity distribution in the annular stenosied catheterized artery at Re=60.
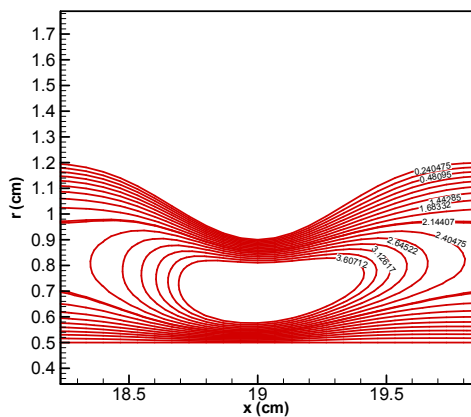
Also, the effect of inline stenosis in the blood artery on the blood velocity vector in the artery was presented in **Fig.12.** The results show that the stenosis height increased with decrease the artery cross section area and leads to increase the velocity in a neck region of the middle region and decrease the velocity value until to reach the zero velocity value in all cases.

(i) 0% Stenosis

Fig.12 Effect of number of stenosis on the velocity factor at Re=60.

(ii) 8% Stenosis

Fig.13. presented the effect of stenosis high on the shear stress distribution. The results show that with increased the stenosis height, the shear stress profile will began to modulate and increased the shear stress lines towered the artery center. Also the increased the stenosis height will lead to activate the shear stress along the catheter wall.

(iii) 16% Stenosis

(iv) 30% Stenosis

(v) 40% Stenosis

(vi) 50% Stenosis

Fig.13 Effect of stenosis high percent on the blood shear stress distribution in the annular stenosied catheterized artery at Re=60.
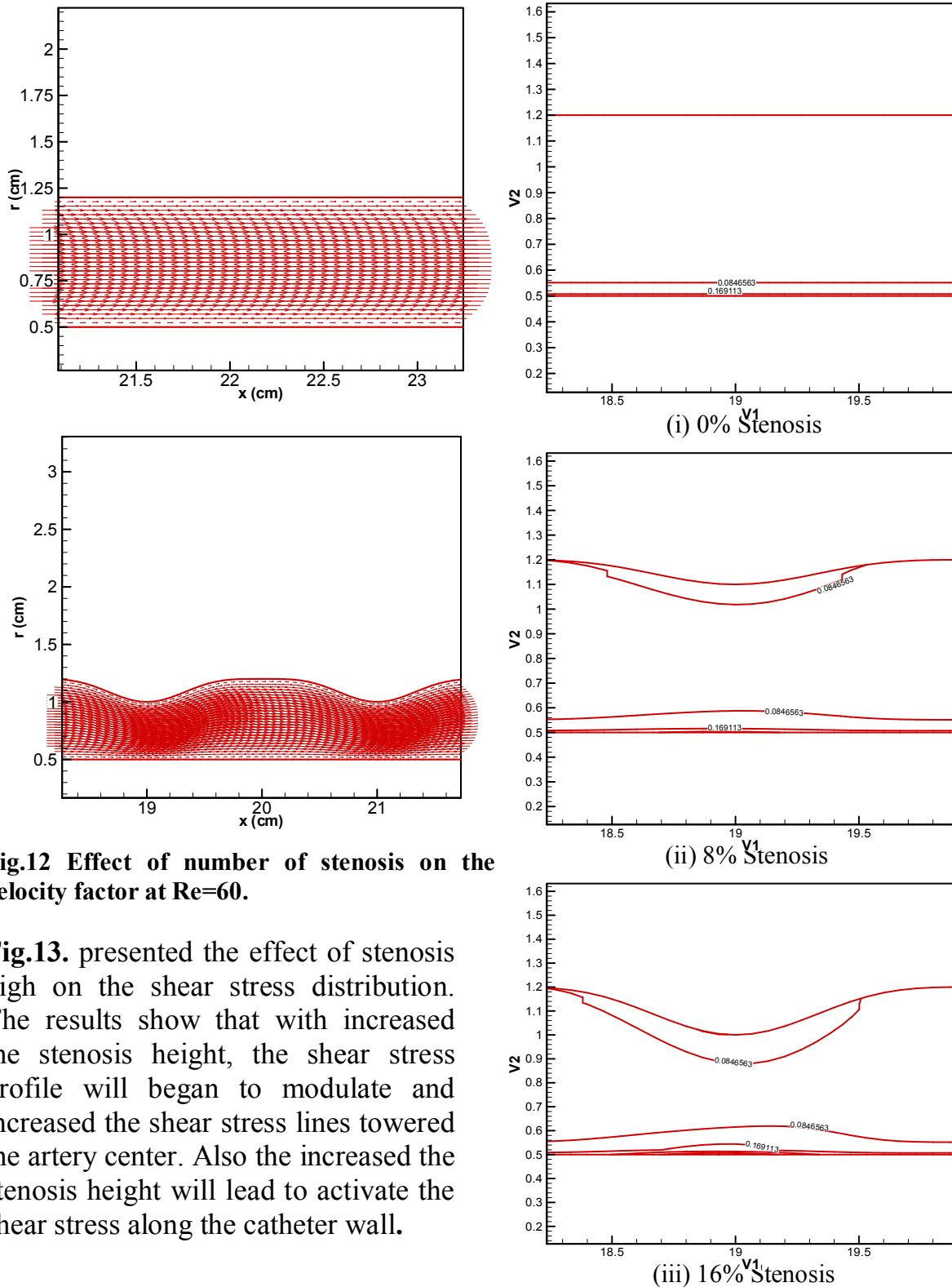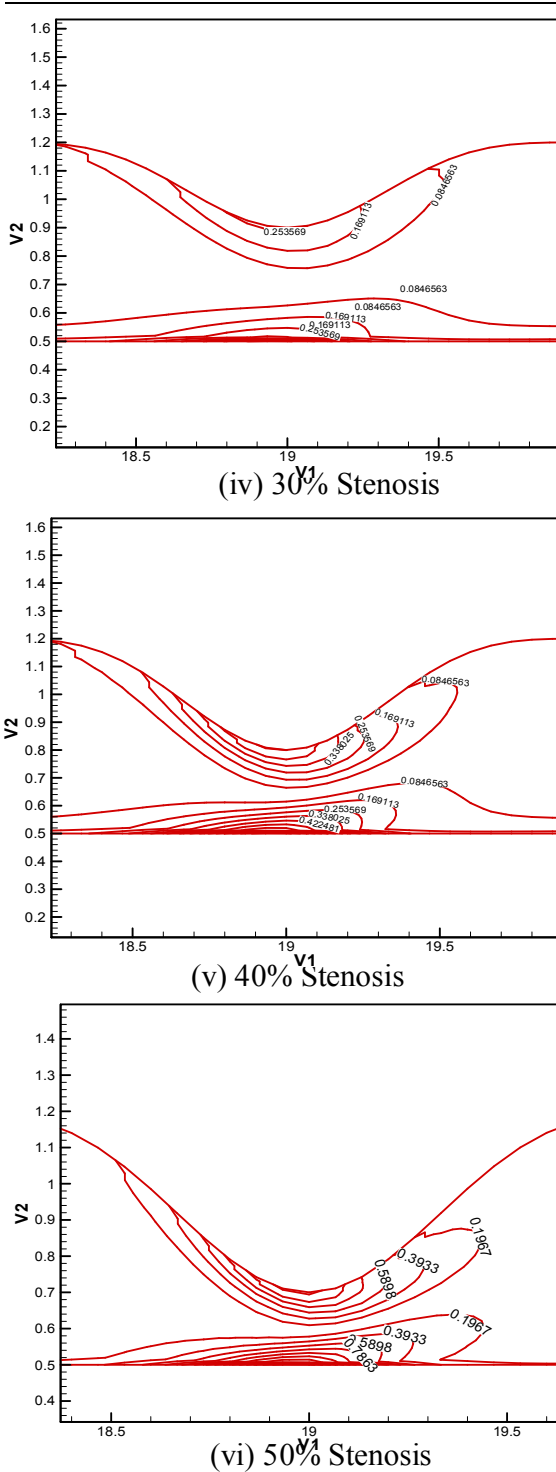
Finally, two cases of the stenosis heights were illustrated in **Fig.14,** to present the blood streamline distribution in the annular stenosied catheterized artery. It shows that the increasing of stenosis heights will increase the blood streamline distribution lines and its values in the middle region of the stenosis this indicate the increased the dynamic velocity of blood flow in this region.

(i) 8% Stenosis

(ii) 50% Stenosis
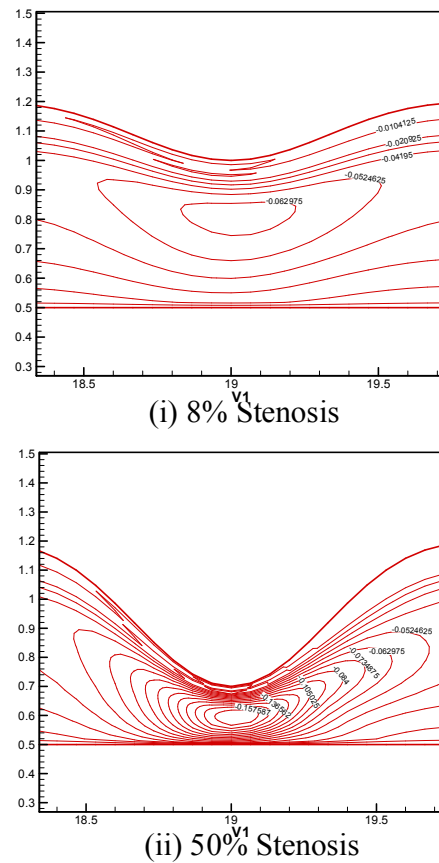
Fig.14 Effect of stenosis high percent on the blood streamline distribution in the annular stenosied catheterized artery at Re=60.

4. Conclusion

From the above discussion, it is clear that the Reynolds number, ratio of maximum stenosis height and normal artery radius and number of stenosis are the strong parameters influenced on the blood flow and heat transfer characteristics in the cooling catheter process was considered in this study. From the numerical results it is observed that:

1. The presence of a single stenosis in the path of the blood flow will case to increasing the maximum velocity that located in the center of the artery by (36%), and increasing the wall shear stress along the artery wall by (55%) but with a percent of (35%) along the cooling catheter wall, and increased the dimensionless flow impedance by (68%), finally increasing the Nusselt number by (36%) as compared with no stenosis artery.

2. The presence of multi stenosis will increase the magnitude of velocity, flow impedance, shear stress, Nusselt number and friction factor in the middle region of the stenosis.

3. The effect of stenosis height and number of stenosis is reduces the blood flow rate. In view of these arguments, the friction factor increased by 52% and Nusselt number increased by 43% with increased the stenosis height from 0 to 16.5%.

References

[1] Bijendra S., J., Padma, B.K., Joshi, 2010, Blood Flow through an Artery Having Radially Non-Symmetric Mild Stenosis, Applied Mathematical Sciences, Vol. 4, no. 22, pp.1065-1072.

[2] Easthope, P., D., Brooks, 1980, A comparison of rheological constitutive functions for whole human blood, Biorheology, Vol.17, 235–247.

[3] Geeta and S. U. Siddiqui, (2016), Analysis of Unsteady Blood Flow through Stenosed Artery with Slip Effects, International Journal of Bio-Science and Bio-Technology Vol.8, No.5 (2016), pp. 43-54.

[4] Haldar, K., 1985, Effects of the shape of stenosis on the resistance to blood flow through an artery. Bulletin of Mathematical Biology, Vol. 47, No.4, pp. 545-550.

[5] Horng, T.L., W.L Lin, C.T. Liauh, T.C. Shih, 2007, Effects of pulsatile blood flow in large vessels on thermal dose distribution during thermal therapy, Med. Phys., 34(4): 1312-1320.

[6] Ismail, Z., Abdullah, I., Mustapha, N. Amin, N., 2007, A power-law model of blood flow through a tapered overlapping stenosed artery, Applied Mathematics and Computation, Vol. 195, No. 2, pp. 669-680.

[7] Jehhef K. A. and Abdulhassan A. Karamalla, (2015), Applications of Nanofluids for Cooling Blood Mimic Fluids, Ph.D. Thesis, Mechanical Engineering, University of Technology, Baghdad, Iraq.

[8] Jinlan H., G. Holt, R. O. Cleveland, R. A. Roy, 2004, Experimental validation of a tractable numerical model for focused ultrasound heating in flow-through tissue phantoms, Boston University, Department of Aerospace and Mechanical Engineering.

[9] Joshi, P., A. Pathak, B. Singh, 2011, Effect of blood flow in a composite stenosed artery, Varahmihir J. Math. Sci.

[10] Kapur, J. N., 2006, Mathematical Models in Biology and Medicine, Affiliated East-West Press, New Delhi.

[11] Mandal, P. K. 2005, an unsteady analysis of non-Newtonian blood flow through tapered arteries with a stenosis. International Journal of Non-Linear Mechanics, Vol. 40, pp. 151-164.

[12] Mohammed A. Al-Rawi, (2006): "Computational Hemodynamics and Blood Flow through an Axisymmetric Arterial Stenosis", M.Sc. Thesis, Mechanical Engineering Department, University of Technology, Baghdad, Iraq.

[13] Muthu, B. V. Rathish K., Pefyush C, 2008, a Study of Micropolar Fluid in an Annular Tube with Application to Blood Flow, India. J.

of Mech. in Medicine and Biology Vol. 8, No. 4, 561–576.

[14] Nidhi, V., R.S. Parihar, 2009, Effects of Magneto-Hydrodynamic and Hematocrit on Blood Flow in an Artery with Multiple Mild Stenosis, Inter. J. of Applied Mathematics and Computation Vol. 1(1), pp 30-46.

[15] Norzieha, M., N. Amin, 2008, the Unsteady Power Law Blood Flow Through a Multi-irregular Stenosed Artery, MATEMATIKA,, Vol. 24, Number 2, 187-198.

[16] Packirisamy, M., S. Ion, Rakheja, S., 2006, Modeling of Blood flow through multi-stenosis arteries, Industrial Electronics, IEEE International Symposium on (Volume:4)

[17] Perktold, K., R. Peter, M. Resch, 2008, Pulsatile non-Newtonian blood flow simulation through a bifurcation with an aneurism, Biorheology, 26, 1011–1030.

[18] Pontrelli, G., 2001, Blood flow through an axisymmetric stenosis, Proc Instn Mech Engrs Vol 215 Part H, H01300.

[19] Sreenadh, S., A. R. Pallavi, B. Satyanarayana, 2011, Flow of a Casson Fluid through an Inclined Tube of Non-uniform Cross Section with Multiple Stenoses, Advances in Applied Science Research, 2 (5): 340-349.

[20] Srikanth, D., 2011, Steady Polar Fluid Flow in a Multiple Constricted Annulus - Catheter Effects, Department of Applied

Mathematics, Defense Institute of Advanced Technology Deemed University.

[21] Srivastava, V. P., 2002, Particulate suspension blood flow through stenotic arteries: Effects of hematocrit and stenosis shape, Indian J. Pure Appl. Math., 33, 1353-1360.

[22] Tashtoush, B., A. Magableh, 2007, Magnetic Field Effect on Heat Transfer and Fluid Flow Charecteristics of Blood Flow in Multi-Stenotic Arteries, Heat and Mass transfer. 35: 125–131.

[23] Thompson J. F., Thomas F. C., and Mastin C. W., "Automatic Numerical Generation of Body Fitted Curvilinear Coordinate System For Field Containing Any Number of Arbitrary Two Dimensional Bodies", J. of computational Physics, Vol. 15, P. 299-319, (1974).

[24] Tu, C., M. Deville, 1996, Pulsatile flow of non-Newtonian fluid through arterial stenosis, J. Biomech, 29, 899–908.

[25] Varun Kumar Tanwar1, N. K. Varshney1 and Raja Agarwal2, Effect of body acceleration on pulsatile blood flow through a catheterized artery, Advances in Applied Science Research, 2016, 7(2):155-166

[26] Verma, S. R., "Mathematical Modeling of Bingham Plastic Model of Blood Flow through Stenotic Vessel", International journal of Engg. Research and Applications, vol. 4, no. 12, (2014), pp. 11-17.

[27] Versteeg, H.K., and Malalasekera, W., 1995, an introduction to computational fluid dynamics-the finite volume method", Longman group Ltd. 9 (7): 253-263.

[28] Walburn, F., D. Schneck, 1976, A constitutive equation for whole human blood, Biorheology, 13, 201–210.

[29] Wang, Y. and Komori, S., "Simulation of the subsonic flow in a High-speed centrifugal compressor Impeller by the pressure-Based Method", Proc. Instn. Mech. Engs., Vol. 212, Part A, Pp. 269-282, (1998).

[30] Yilmaz, F. and M. Y. Gundogdu, 2008, A critical review on blood flow in large arteries; relevance to blood rheology, viscosity models, and physiologic conditions., Korea-Australia Rheology J. Vol. 20, No. 4, December, pp. 197-211.

Nomenclatures

C_p blood specific heat
D   stenosis length. viscosity, Pa.s.
E   calculation error.
f   Darcy friction factor .
h   heat transfer coefficient, $W/m^2.K$.
H   Hematocrit expressed as a percentage, %.
i   number of nodes along x-axis.
j   number of nodes along r-axis.
J   Jacobian of direct transformation.
k   thermal conductivity, W/m.K.
L   artery axial length, m.
m   power-law consistency coefficient, $Pa.s^n$
n   power law flow behaviour index.
p   pressure, pa
R   dimensional radius=r/R_o.
r   radial distance from pipe centerline, m.
Re_b blood Reynolds Number
r_c radial coordinate = $(r–R_i)/(R_o–R_i)$.
RF   relaxation factor
R_i inner diameter of annulus, m.
R_{min} minimum radius of stenosis, m.
r_o center of maximum velocity, m.
R_o outer diameter of annulus, m.
T_c local cooling catheter surface temperature, ^oC.
T_b local body surface temperature, ^oC.
T_{in} blood inlet temperature, $^o C$.
u   velocity component in x-direction, m/s.
U_o bulk axial velocity, m/s.
v   velocity component in r-direction , m/s.
x   axial distance along artery, m.
X   Non-dimensional viscosity.

Greek letters

μ dynamic viscosity, Pa.s.
μ_{eff} effective dynamic viscosity, Pa.s.
α, β, γ Transformation parameter
γ Shear rate, 1/s.
ρ density, kg/m^3
μ_P viscosity of plasma, cP.
τ shear stress, N/m^2 .
ϕ dependent variable.
ω vorticity, 1/s.
ψ stream function, m^2 /s.
ζ, η Coordinate in the domain
Λ Material parameter

دراسة عددية لجريان وانتقال حرارة الدم في شريان متعدد التصلبات بوجود القسطرة

د. كاظم عودة جحف
قسم المكائن والمعدات
معهد تكنلوجيا- بغداد, الجامعة التقنية الوسطى

الخلاصة

تم اعتماد نموذج المائع الغيرنيوتيني لنمذجة جريان الدم في شريان متعدد التضيقات عند النقاط التالية ($x/L = 0.6$, $0.7, 0.8$ and 0.9) ولقيم عدد رينولدز هي ($60, 80, 100, 120$) مع وجود قسطار مركزي داخل الشريان للتبريد الداخل شرياني. وان النموذج المستخدم لتحليل لزوجة الدم هو نموذج كروس. حيث تم اعتماد فرضيات الجريان المستقر والطباقي وثنائي الابعاد المتناظر حول المحور. وايضا تم استخدام المعادلات الحاكمة للحركة وانتقال الحرارة بدلالة اجهاد القص اللزج والظروف الحدية لنظام الاحداثيات الاسطوانية. حيث تم اولا استخدام التحويل باستخدام نظام التحويل الاحداثي القطري ومن ثم تم استخدام طريقة الفروق المحددة للتحليل العددي المعتمد على تقريب الفروق المركزية على النقاط غير المنتظمة. اظهرت النتائج العددية المتحصلة بدلالة خواص جريان وانتقال الحرارة للدم ان قيم معامل الاحتكاك يزداد بمقدار 52% وعدد نسلت بمقدار 43 % عند زيادة ارتفاع التضيق من 0 الى 16.5 %, وكذلك فان زيادة ارتفاع التضيق يؤدي الى زيادة السرعة المحورية للدم في منطقة التضيق وزيادة قيم الممانعة اللابعدية وقيم اجهاد القص على كلاً من جدار الشريان وجدار القسطار. وان وجود عدة تضيقات في جدار الشريان تؤدي الى زيادة الممانعة لتدفق الجريان.

الكلمات المفتاحية: نموذج كروس، تجلطات متعددة، الشريان المتجلط، جريان الدم.